31st Congress of the International Council of the Aeronautical Sciences
Belo Horizonte, Brazil; September 09-14, 2018

NUMERICAL STUDY OF VARIABLE CAMBER WING EFFECT ON AERODYNAMIC PERFORMANCE FOR LONG RANGE CIVIL AIRCRAFT

Qian Guangping1*, Wu Dawei, Ma Chao****
***Shanghai Aircraft Design and Research Institute**

Keywords: *Variable camber; Trailing edge; Mach number; Pressure distribution; Long range*

Abstract

In order to increase the aerodynamic effectiveness of the long range wide body transport jet with the change of lift, mach number and altitude ,the technology of trailing edge variable camber wing which can change wing's shape by the deflection of flap ,aileron and spoiler depending on the flight condition has been applied to civil aircraft. Taking the wing of a representative long range wide body aircraft as a case study, the effects of variable camber of wing's aerodynamic performance and pressure distribution are investigated by the mean of CFD. Meanwhile, the drag coefficient and the lift-to-drag ratio with the variable of wing's chamber according to the different mach number and lift coefficient are analyzed. By applying surrogate model, the relationship between wing's camber and lift-to-drag ratio under the different flight condition are established. Finally, the fuel economy are built when applying wing variable camber in different flight range. The study shows that the optimization method can achieve best aerodynamic performance at given lift coefficient and mach number, result in aerodynamic performance improvement and fuel consuming decrease. It can make the aircraft fly in the fixed cruise altitude without stepped cruise.

1 General Introduction

Recently, as the increasing competition of civil aircraft market, many domestic and overseas institutes make great efforts to improve airplane's economy through all kinds of advanced technology. Among of these technology is variable camber function of wing's trailing edge which is introduced in long range wide-body aircraft, such as Boeing 787 and Airbus 350. It can reduce B787 aircraft's weight about 340~450kg adopting this new function. On the other hand, A350 introduces some technology of drag reduction in cruise, load control and assistant low speed function by moving wing's trailing edge control surfaces. There are no many domestic researches concerning variable camber wing function, but focusing on the machine and airfoil's aerodynamics of variable camber.

This paper presents some numerical study about variable camber wing effect on high speed aerodynamic performance for long range wide-body airplane giving the rule of drag and lift-drag ratio as variable camber wing in different mach number and lift coefficient. Finally, it shows the fuel economy's variation according to the lift/drag polar curve of variable camber wing.

The variable camber function is achieved through moving flaps, flaperon and spoilers while the rotation angle is from minus 1.5 degrees to 1.5 degrees. The spoilers' movement follows flaps' rotation assuring that there is no gap between spoilers and flaps.

2 Computational methodology

2.1 Governing equation

2.1.1 Full-potential equation

The unsteady full-potential equation written in a body fitted coordinate system is given by

$$(\rho J)_\tau + (\rho U J)_\xi + (\rho V J)_\eta + (\rho W J)_\zeta = 0 \qquad (1)$$

where ρ is density, U, V, and W are the contravariant velocity components in the ξ, η, and ζ, directions, τ means time, and J is Jacobian. Eq. (1) is solved by the time-accurate approximate factorization algorithm and internal Newton iterations; body conditions and wake conditions are implicit embedded.

2.1.2 Boundary layer equation

The original system of differential equations, which governs the gas flow in the three-dimensional boundary layer has the form:

$$\left.\begin{aligned}
&\frac{\partial}{\partial x}(\rho u h_2 \sin\theta) + \frac{\partial}{\partial z}(\rho w h_1 \sin\theta) + \frac{\partial}{\partial y}(\rho v h_1 h_2 \sin\theta) = 0 \\
&\rho\frac{u}{h_1}\frac{\partial u}{\partial x} + \rho\frac{w}{h_2}\frac{\partial u}{\partial z} + \overline{\rho v}\frac{\partial u}{\partial y} - \rho k_1 u^2 \cot\theta + \rho k_2 w^2 \csc\theta + \rho k_{12} uw = \\
&\quad = -\frac{\csc^2\theta}{h_1}\frac{\partial p}{\partial x} + \frac{\csc\theta\cot\theta}{h_2}\frac{\partial p}{\partial z} + \frac{\partial}{\partial y}(\mu\frac{\partial u}{\partial y} - \overline{\rho u' v'}) \\
&\rho\frac{u}{h_1}\frac{\partial w}{\partial x} + \rho\frac{w}{h_2}\frac{\partial w}{\partial z} + \overline{\rho v}\frac{\partial w}{\partial y} - \rho k_2 w^2 \cot\theta + \rho k_1 u^2 \csc\theta + \rho k_{21} uw = \\
&\quad = -\frac{\cot\theta\csc\theta}{h_1}\frac{\partial p}{\partial x} + \frac{\csc^2\theta}{h_2}\frac{\partial p}{\partial z} + \frac{\partial}{\partial y}(\mu\frac{\partial w}{\partial y} - \overline{\rho w' v'})
\end{aligned}\right\} \qquad (2)$$

where $\overline{\rho v} = \rho v + \overline{\rho' v'}$.

The coordinate *y* is directed along the normal to the wing surface, the variables *x, z* govern the system of non-orthogonal coordinates with angle $\theta(x,z)$ between them on the surface, *u,v,w* - are the components of the velocity vector along the coordinates *x,y,z*, ρ- is the density, *p* - is the pressure, μ - is the dynamic viscosity coefficient, $h_1 = \partial s_1/\partial x, h_2 = \partial s_2/\partial x$ are the metric coefficients.

The parameters k_1, k_2, k_{12}, k_{21} characterize curvature of coordinate lines *z*=const, *x*=const. has form:

$$k_1 = \frac{1}{h_1 h_2 \sin\theta}\left[\frac{\partial}{\partial x}(h_2\cos\theta) - \frac{\partial h_1}{\partial z}\right]$$

$$k_2 = \frac{1}{h_1 h_2 \sin\theta}\left[\frac{\partial}{\partial z}(h_1\cos\theta) - \frac{\partial h_2}{\partial x}\right]$$

$$k_{12} = \frac{1}{\sin\theta}\left[-\left(k_1 + \frac{1}{h_1}\frac{\partial\theta}{\partial x}\right) + \cos\theta\left(k_2 + \frac{1}{h_2}\frac{\partial\theta}{\partial z}\right)\right]$$

$$k_{21} = \frac{1}{\sin\theta}\left[-\left(k_2 + \frac{1}{h_2}\frac{\partial\theta}{\partial z}\right) + \cos\theta\left(k_1 + \frac{1}{h_1}\frac{\partial\theta}{\partial x}\right)\right]$$

The boundary conditions are as follows:

on the external edge of the boundary layer:

$$y = \delta, \quad u = u_e(x,z), \quad w = w_e(x,z)$$

on the wall:

$$y = 0, \quad u = w = 0 \quad v_w = 0$$

2.2 Viscous-inviscid interaction

For the determination of self-consistent solutions the quasi-simultaneous coupling scheme is used. It allows one to take into account the expected boundary layer response to the chordwise velocity variation while calculating the external flow, and ensures effective and rapid computation of viscid-inviscid interaction including moderate separation regimes.

3 Computational validation

To validate the flowfield computation method, the DLR-F6 model was numerically simulated and compared with the experimental data at CL=0.57. The DLR-F6 model is a twin-engine aircraft model, with a variety of wind-tunnel experiment data and numerical solutions available over years. The nacelle of DLR-F6 is a through flow nacelle. Fig. 1 shows the variation of CL with the number of grid points for the DLR-F6 wing-body/nacelle, indicating that the 600000 grid points are adequate for this simulation. The computational grid for the DLR-F6 wing-body/nacelle (600000 grid points) is presented in Fig. 2.

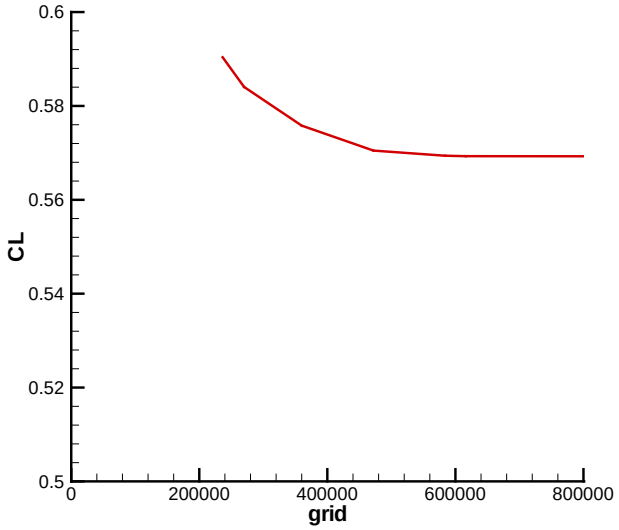

Fig. 1 The variation of CL with the number of grid points.

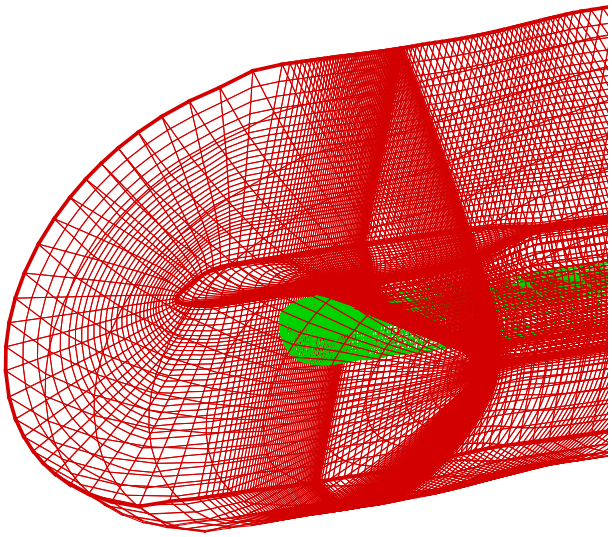

Fig. 2 DLR-F6 wing-body/nacelle grid.

The wing pressure distributions from the present computation and experiments are shown in Fig. 3, respectively, with Ma=0.75, CL= 0.4 and Reynolds number of 3×106 based on the mean aerodynamic chord. The lift-to-drag characteristics between the calculations and experiments are shown in Fig. 4.The simulated results are in excellent agreement with the experiments, showing that the grid generation strategy and numerical method are adequate for this case. Thus, overall, the simulation gives a satisfactory prediction of pressure distribution, lift-to-drag characteristics and is therefore considered to be a satisfactory basis for determining simulations.

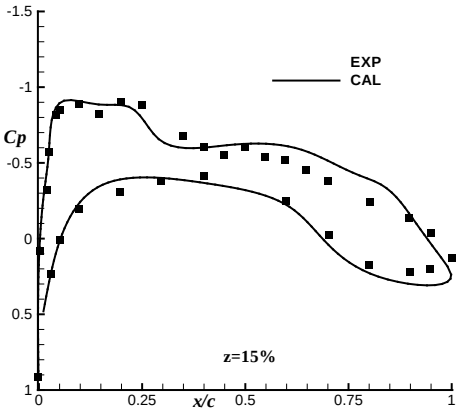

(a) at z=15%

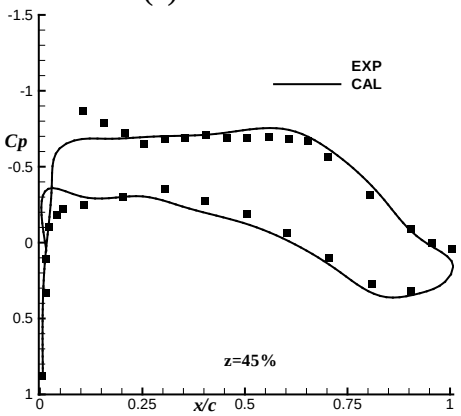

(b) at z=45%

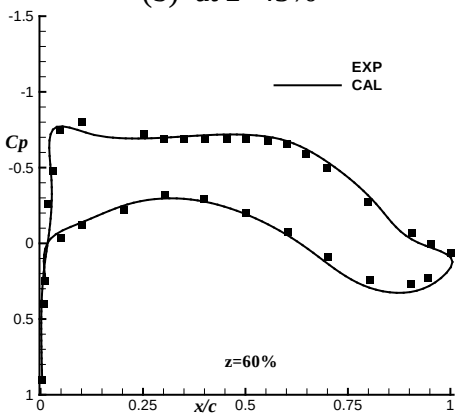

(c) at z=60%

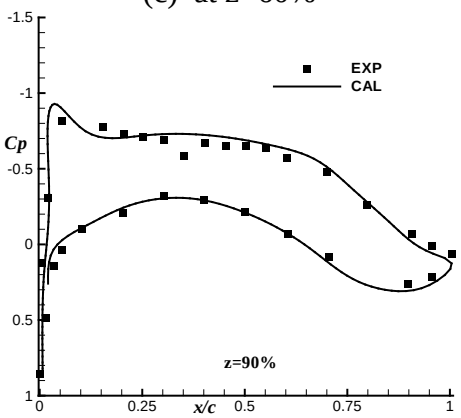

(d) at z=90%

Fig. 3 Wing surface Cp comparison at Ma=0.75.

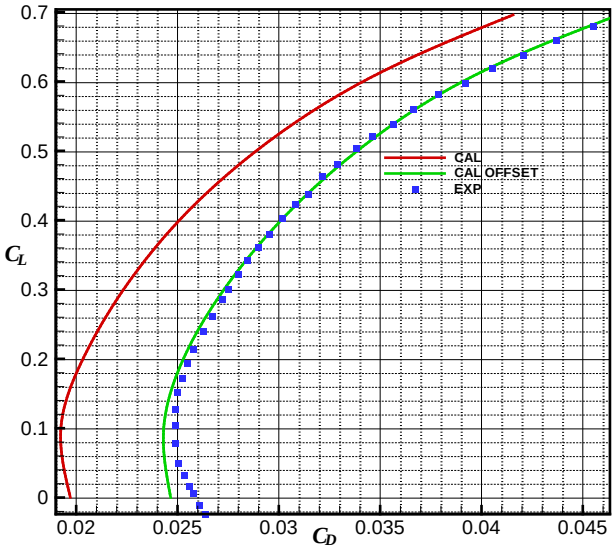

Fig. 4 Lift-to-drag characteristics comparison at Ma=0.75.

4 Results and discussion

Taking a long range wide-body aircraft for instance, a numerical simulation is performed. Comparison analysis is conducted at the mach number of 0.80,0.85,0.89 and the lift coefficient of 0.50.

4.1 Ma=0.85

The numerical results of variable camber wing's aerodynamics in classic mach number 0.85 are presented in Fig. 5. It declares the lower drag as the smaller trailing edge camber by moving flaps upwards in the case of low lift coefficient. Meanwhile the location of the maximum lift-to-drag ratio turns left indicating the smaller camber, the larger moving range. On the other hand, it shows that the lower drag as the larger trailing edge camber by moving flaps downwards in the case of high lift coefficient. Meanwhile the location of the maximum lift-to-drag ratio turns right indicating the larger camber, the larger moving range. So it is suitable to adopt large camber wing in high lift coefficient, otherwise small camber wing in low lift coefficient. However, the maximal lift-to-drag ratio appears in the configuration of original wing indicating which is the optimization configuration in the case of classic cruise.

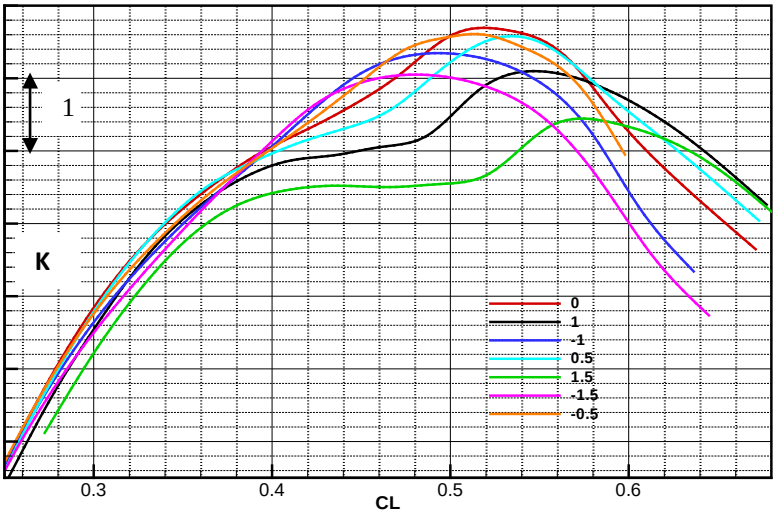

Fig. 5 Aerodynamics comparison at Ma=0. 85 in different rotation angle

Also shown in Fig. 6 and Fig. 7 are the comparison of wing's pressure distribution and contour at classic cruise mach number 0.85, lift coefficient 0.5 adopting variable camber function. The results indicate that it has obvious effect on pressure distribution for supercritical wing even if there is a little movement of trailing edge. The location of shock wave moves aft and the suction peak of leading edge descends when the trailing edge moves downwards increasing wing's camber. On the other hand, the shock wave position moves ahead and the suction peak of leading edge ascends when the trailing edge moves upwards reducing wing's camber. Comparing to original wing, it enhances the strength of shock wave and increases drag obviously whether increasing camber or reducing camber which is consistent with the results in Fig. 5 .

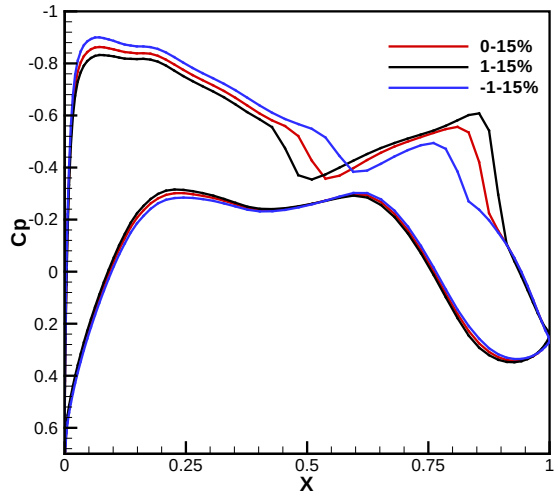

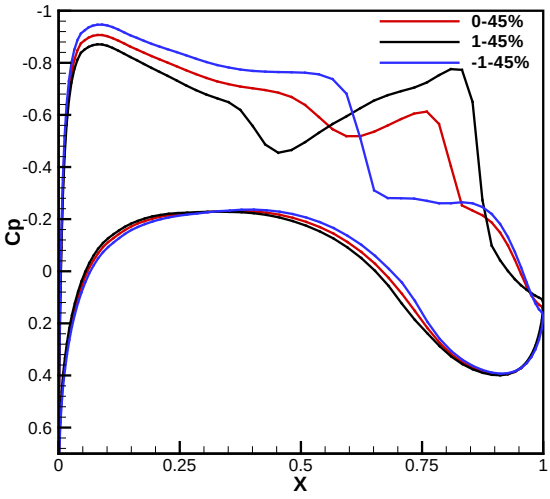

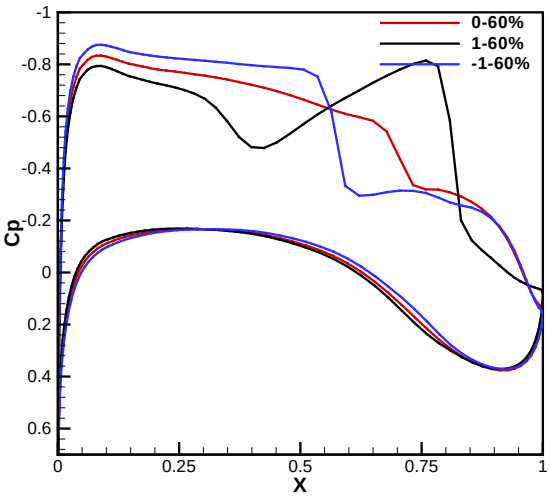

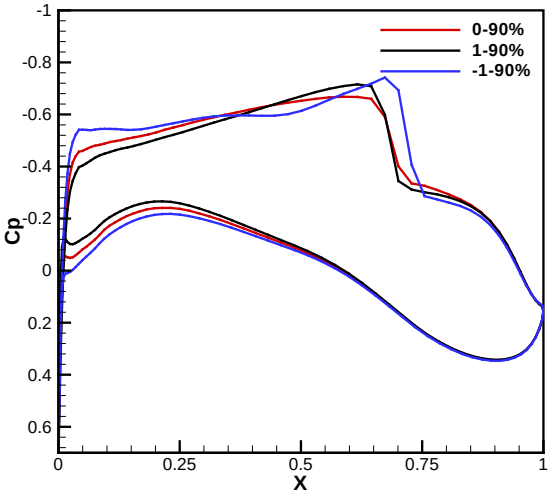

Fig. 6 Pressure distribution comparison at Ma=0. 85 CL=0.5 in different rotation angle

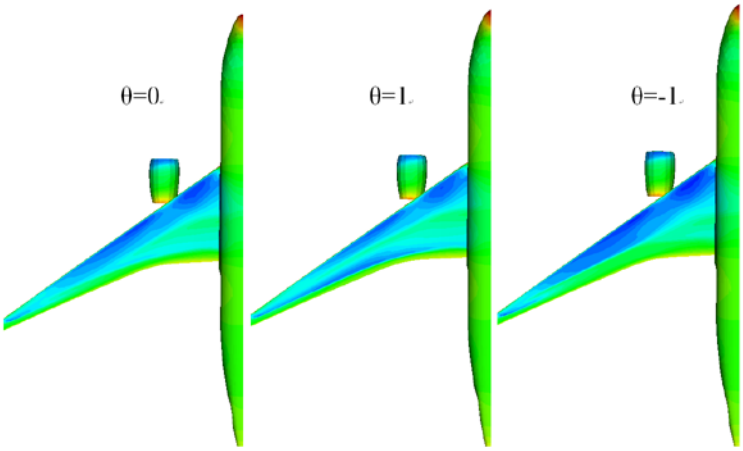

Fig. 7 Pressure contour comparison at Ma=0. 85 CL=0.5 in different rotation angle

4.2 Ma=0.80

Fig. 8 shows the numerical results of variable camber wing's aerodynamics at Ma=0. 80.The location of the maximum lift-to-drag ratio turns right indicating the larger camber, the higher lift-to-drag ratio according to the results in Fig. 4. We conclude that it is suitable to adopt large camber wing at Ma=0.80 that is under the classic mach number of 0.85, especially in high lift coefficient which can acquire much more benefits .

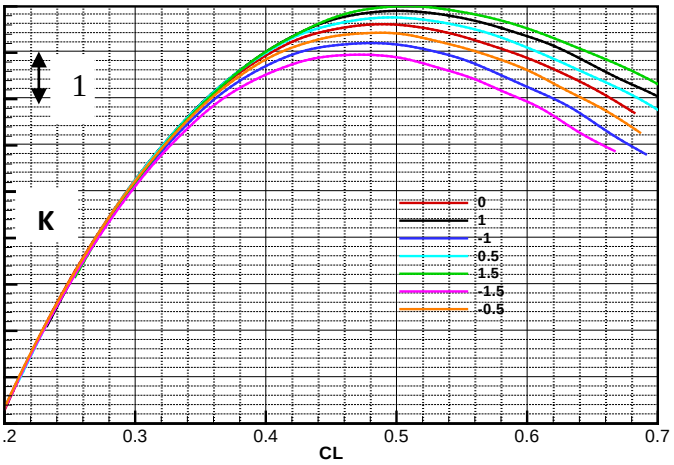

Fig. 8 Aerodynamics comparison at Ma=0. 80 in different rotation angle

Also shown in Fig. 9 and Fig. 10 are the comparison of wing's pressure distribution and contour at Ma= 0.80, lift coefficient 0.6 adopting variable camber function. The results indicate that the location of shock wave moves ahead, the strength of shock wave decreases and the suction peak of leading edge descends when the trailing edge moves downwards increasing wing's camber. On the other hand, the shock wave position moves aft, the strength of shock wave increases and the suction peak of leading edge ascends when the trailing edge moves upwards reducing wing's camber which is consistent with the results in Fig. 8 .

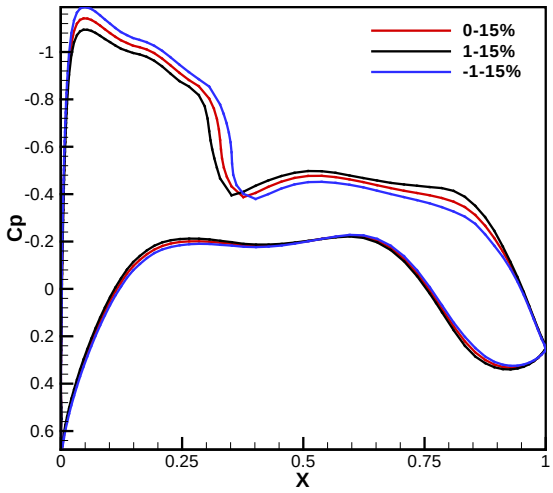

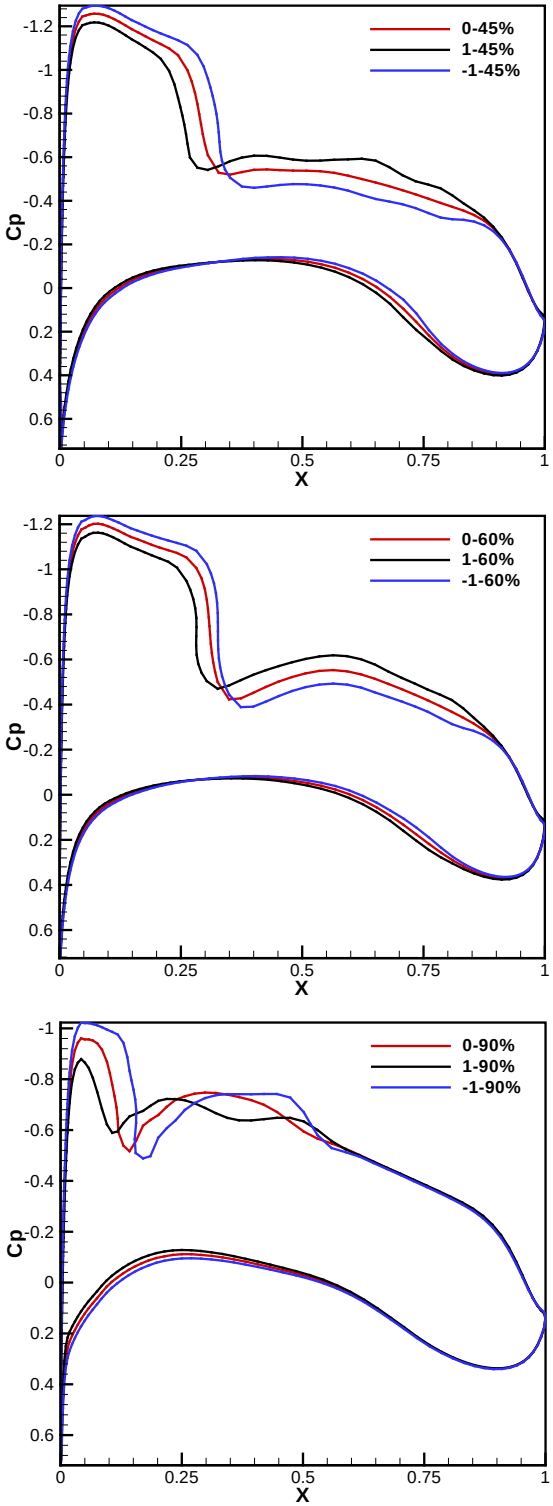

Fig. 9 Pressure distribution comparison at Ma=0. 80 CL=0.6 in different rotation angle

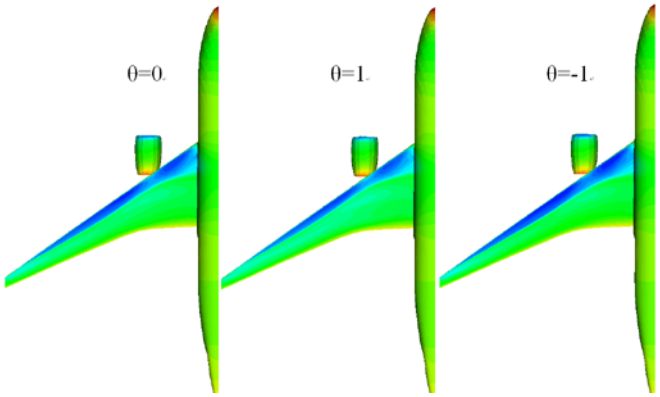

Fig. 10 Pressure contour comparison at Ma=0. 80 CL=0.6 in different rotation angle

4.3 Ma=0.89

The numerical results of variable camber wing's aerodynamics at Ma=0.89 above the classic mach number of 0.85 are presented in Fig. 11. It proclaims the lower drag as the smaller trailing edge camber and the location of the maximum lift-to-drag ratio turns left by moving flaps upwards in the case of lift coefficient range. We conclude that it is suitable to adopt small camber wing at Ma=0.89 that is above the classic mach number of 0.85, lift coefficient ranging from0.2 to 0.6, especially in low lift coefficient which can acquire much more benefits .

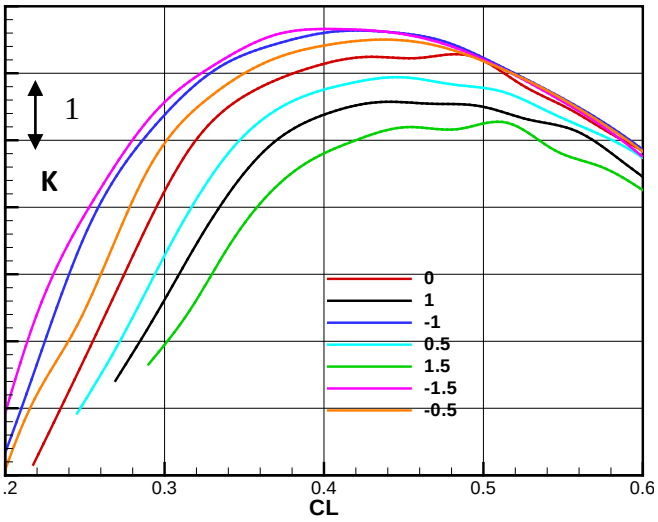

Fig. 11 Aerodynamics comparison at Ma=0. 89 in different rotation angle

Also shown in Fig. 12 and Fig. 13 are the comparison of wing's pressure distribution and contour at Ma= 0.89, lift coefficient 0.4 adopting variable camber function.
The results indicate that the location of shock wave moves ahead, the strength of shock wave decreases and the suction peak of leading edge ascends when the trailing edge moves upwards decreasing wing's camber. On the other hand, the shock wave position moves aft, the strength of shock wave increases and the suction peak of leading edge descends when the trailing edge moves downwards increasing wing's camber which is consistent with the results in Fig. 11 .

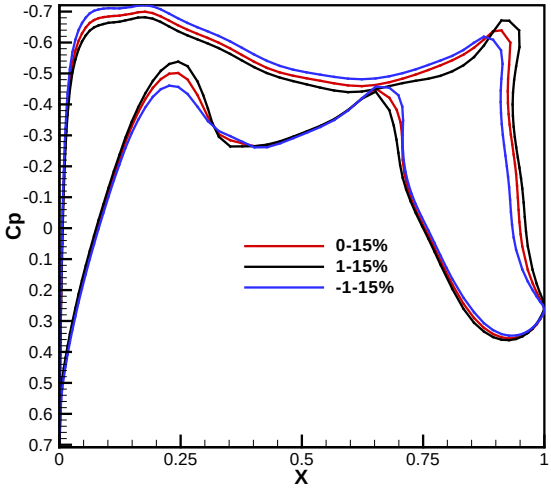

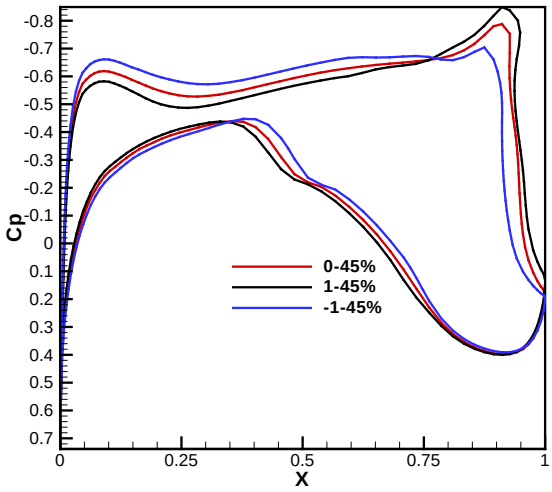

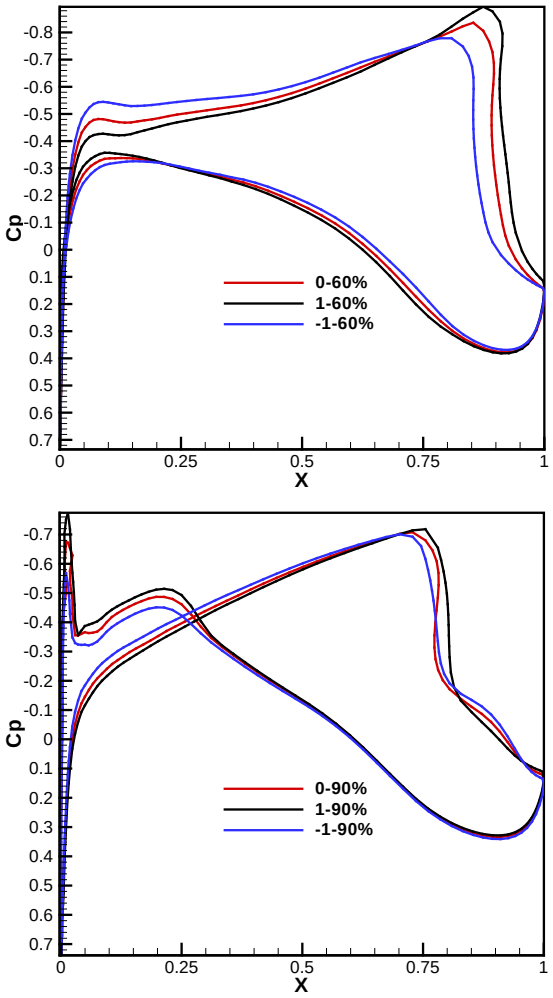

Fig. 12 Pressure distribution comparison at Ma=0. 89 CL=0.4 in different rotation angle

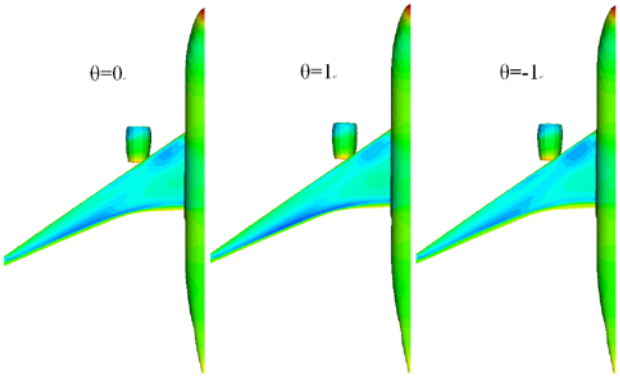

Fig. 13 Pressure contour comparison at Ma=0. 89 CL=0.4 in different rotation angle

4.4 Fuel performance

It can gain the highest aerodynamic efficiency in the case of every flight condition to meet maximum fuel consumption economy through moving trailing edge control surfaces according to the variation of weight and altitude in climb and cruise.

The block fuel consumption adopting variable camber function saves about 1% at the range of 3500nm and 6500nm comparing to original configuration.

5 Conclusions

In this work, we presented the numerical simulation results of variable camber wing effects on long range wide body aircraft aerodynamic characteristics. The following conclusions are drawn.

1) It is suitable to adopt large camber wing by moving trailing edge control surfaces downwards at mach number that is under the classic mach number.

2) It is suitable to adopt small camber wing by moving trailing edge control surfaces upwards at mach number that is above the classic mach number.

3) The block fuel consumption saves about 1% adopting variable camber function .

6 Contact Author Email Address

My email address: qianguangping@comac.cc

Copyright Statement